Reflection from Bound Microbubbles at High Ultrasound Frequencies

Olivier Couture, Michael R. Sprague, Emmanuel Cherin, Peter N. Burns, and F. Stuart Foster

***Abstract*—Targeted contrast agents and ultrasound imaging are now used in combination for the assessment and tracking of biomarkers in animal models *in vivo*. These applications have triggered interest in the understanding and prediction of the ultrasound echoes from contrast agents attached to cells. This study describes the reflection enhancement due to microbubbles bound on a gelatin surface. The reflection enhancement was measured using ultrasound pulses at high frequency (40 MHz) and low pressure (38 kPa peak-negative-pressure) allowing a linear approximation to be applied. The observed reflection coefficient increased with the number of microbubbles, until reaching saturation at 0.9 when the surface coverage fraction was 35%. A multiple scattering model assuming that the targeted microbubbles are confined within an infinitesimally thin layer appeared suitable in predicting the reflection coefficient even at very high surface densities. These results could permit the optimization of the sensitivity of high-frequency ultrasound to targeted contrast agents.**

I. Introduction

A better understanding of the genetic and proteomic mechanisms of diseases like atherosclerosis and cancer has created an opportunity for new treatments based on molecular medicine. However, selection of proper molecular targets for therapy is partly limited by the lack of information about their expression in living patients. Targeted microbubbles [1], in combination with ultrasound imaging, has allowed molecular imaging of angiogenesis [2]–[9], inflammation [10], [11], and thrombus [12], [13] in animal models. Optimization of these agents requires improvements in the specificity of targeting, as well as sensitivity of the ultrasound system to the bound microbubbles. Past improvements in the contrast derived from microbubbles have been obtained using pulse sequences, such as pulse-inversion, derived from a better understanding of the bubble's behavior [14]. For this reason, the acoustic response of free microbubbles in aqueous media has been modeled extensively [15]. For ultrasound molecular imaging, it is of interest to describe the acoustic behavior of microbubbles when they are bound to cells through targeting ligands.

Manuscript received February 26, 2008; accepted October 20, 2008. The authors thank the National Cancer Institute for the funds from the Terry Fox Foundation, the Canadian Institutes for Health Research, the Ontario Research and Development Challenge Fund, and VisualSonics Inc for supporting this work.

The authors are with Imaging Research, Sunnybrook Health Sciences Centre/Department of Medical Biophysics, University of Toronto, Toronto, Canada (e-mail: olicou@gmail.com).

O. Couture is currently located at Laboratoire Ondes et Acoustique, Paris, France.

Digital Object Identifier 10.1109/TUFFC.2009.1070

Current models for the behavior of microbubbles in an acoustical field assume isotropic oscillations. This assumption may be less valid when applied to targeted microbubbles because of the inherent asymmetry of the boundary conditions. The effect of a boundary close to the microbubble can be partly compensated through a mirror-image method as demonstrated by Garbin *et al.* [16]. However, microbubbles cannot be assumed to have a spherical shape during oscillation because of the forces applied by the surface and the tethering by the targeting ligands [17]. In addition, contrary to the use of microbubbles for contrast enhancement, targeted microbubbles might accumulate at very high concentrations and form nonrandom patterns, such as when they are aligned on the internal surface of a blood vessel. For instance, it has been demonstrated that several targeted microbubbles can bind to a single cell *in vitro* [7], [18] leading to surface densities potentially surpassing 1000 microbubbles/mm^2. In such conditions, the acoustic response of a population of bound microbubbles cannot be derived from the linear summation of the single-bubble behavior as observed by Lankford [19]. It is thus necessary to consider the effects due to coherent [20] and multiple scattering.

Modeling the acoustic behavior of collections of bound microbubbles can be greatly simplified by assuming linear conditions. Such an assumption allows the use of elementary metrics such as the reflection coefficient and the backscattering coefficient. For sufficiently low incident pressures and excitation frequencies sufficiently far from their resonance peak, microbubbles can be regarded as simple linear scatterers with a frequency-dependent backscattering cross section [21]. Such a simplification is used in this study as a first step in the understanding of the acoustical behavior of bound microbubbles.

The goal of this study is to describe theoretically and experimentally the reflection of high-frequency ultrasound from surfaces covered with different densities of microbubbles. A multiple-scattering model is introduced, and ultrasound experiments performed with bound microbubbles co-registered with a wide-field microscope on a poorly reflecting (gelatin) surface are described.

II. Theory

To predict the reflection coefficient from targeted microbubbles attached to a poorly reflecting surface, the scattering cross section of individual microbubbles must be determined. For bubbles much smaller than the wavelength of the interrogating pulse and for frequencies much

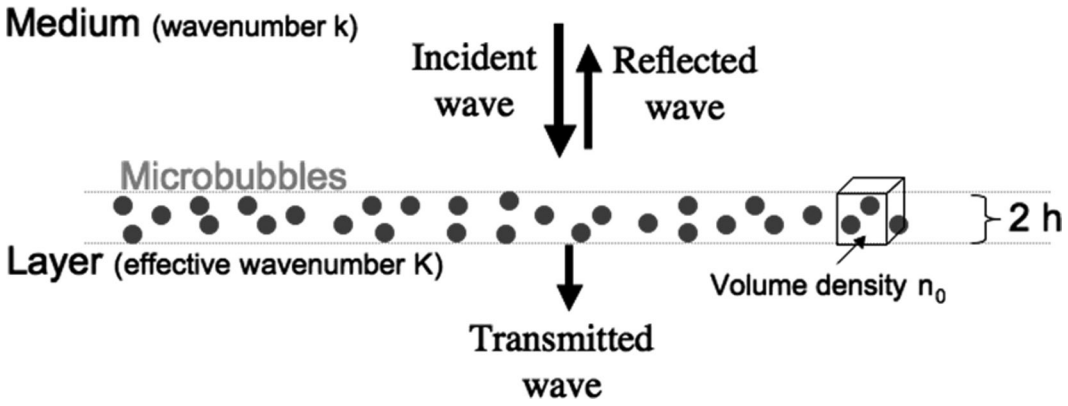

Fig. 1. Layer of scatterers reflecting ultrasound.

larger than the bubble's resonance frequency, the linear-scattering cross-section σ_{lin} can be written very simply as the geometrical cross section [21]

$$\sigma_{\text{lin}} = 4\pi {R_0}^2 \tag{1}$$

where R_0 is the radius of the microbubble.

When single scattering is assumed, the reflection coefficient of a layer of particles can be calculated from the linear sum of the contributions from each particle weighted by the particle size distribution, while taking diffraction into account [20]. However, it is necessary to consider multiple scattering for strong scatterers at high concentrations.

Following Chin [22], multiple scattering can be assumed significant when the secondary scattering ratio (R_{ps}) surpasses about 10%. This ratio is defined as the ratio of the incident intensity to the primary scattering, given by $\sigma_S / {r_{\text{mean}}}^2$, where r_{mean} is the average distance to the nearest particle (calculated in appendix). For particles on a plane, this yields

$$R_{\text{ps}} = \sigma_S / {r_{\text{mean}}}^2 = \sigma_S \Big/ \left(\frac{1}{2\sqrt{n_S}}\right)^2 = 4 n_S \sigma_S = 16\pi n_S {R_0}^2 \tag{2}$$

where n_S is the surface density of the microbubbles.

From (2), the secondary scattering becomes significant for 1 μm-radius microbubbles distributed on a plane when the surface density is about 2000/mm^2.

Many authors have developed models to calculate the effect of multiple scattering on the acoustical properties of a medium [23]–[25]. In particular, Angel and Aristegui [26] described the acoustical reflection of a layer of thickness $2h$ containing particles floating in the same medium that surrounds the layer (Fig. 1). This analysis of multiple scattering was based on a theory proposed by Waterman and Truell [25]. The interest of this model comes from the fact that it derives the reflection coefficient directly from the far-field scattering properties of a single particle. For isotropic and randomly distributed scatterers, an effective wavenumber (K) within the layer can be determined as

$$K^2 = k^2 + 4\pi n_0 f \tag{3}$$

where k is the wavenumber within the medium surrounding the particles, n_0 is the volume concentration of the scatterers, and f is the scattering function of a single scatterer.

The acoustic impedance ratio (Q) is expressed as

$$Q = \frac{K - k}{K + k} \tag{4}$$

and the resulting reflection coefficient is

$$R = \frac{Q e^{-2ikh}}{1 - Q^2 e^{4iKh}} (1 - e^{4iKh}). \tag{5}$$

Adapting the model by Angel and Aristegui [26] for an infinitely thin layer, the thickness $2h$ becomes 0, and the volume density is the surface density divided by the thickness ($n_0 = n_S/2h$). In such a case, the reflection coefficient can be reduced to

$$R \xrightarrow[h \to 0]{} 2\pi i \frac{n_S f}{k} \left(\frac{1}{1 - 2\pi i \frac{n_S f}{k}} \right). \tag{6}$$

This expression of the reflection applies to isotropic scatterers uniformly and randomly distributed on an infinite plane. Any order in the particle positions, which could occur for example when they are closely packed, would likely introduce a crystalline term [27]. The scattering function (f) of a microbubble of radius R_0 can be obtained from the scattered pressures calculated through various models [15], [28], [29]. If the phase can be disregarded, f becomes the square root of the scattering cross section. When the particles are polydisperse, their scattering function is weighted by the size distribution of the particles.

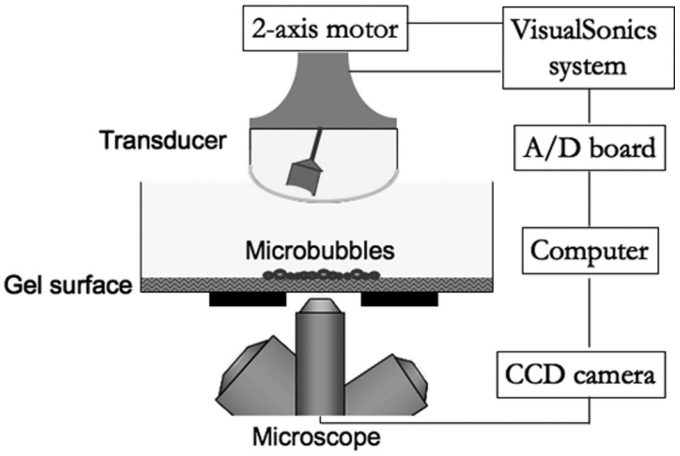

Fig. 2. Experimental setup for the measurement of the reflection enhancement induced by microbubbles bound to a surface. The microscope is used to determine the surface density of microbubbles.

III. Experiment: Material and Methods

The experiment consisted of measuring the change in the reflectivity of a surface due to bound microbubbles.

A gelatin surface immersed in water was used as a model for tissue. Twenty milliliters of a solution of 2% weight/volume gelatin (Sigma-Aldrich Co., St. Louis, MO) was poured into a tissue culture dish. The dishes were left to solidify and dry for about 2 h. Streptavidinated microbubbles (Bracco Research SA, Geneva, Switzerland) were prepared following the protocols of the manufacturer. The avidinated bubbles were then diluted in various amounts of phosphate buffered saline (PBS) down to a 1/1440 of the original concentration and left on ice. Fifteen μL of each concentration of streptavidinated microbubbles were dotted on the gelatin plates (serial dilution). The plates were then inverted and the microbubbles left to interact with the surface for 15 min. The plates were washed with degassed PBS to eliminate the unbound microbubbles and immersed in a water bath for imaging (Fig. 2).

Ultrasound imaging was performed using a Visualsonics Vevo770 (Visualsonics Inc., Toronto, ON, Canada) equipped with a 40 MHz probe (6 mm focal length, 3 mm diameter, −6 dB beam cross section calculated to be 4400 μm^2) focused on the gelatin surface. This system was mounted on top of an inverted optical microscope (Leica, Wetzlar, Germany). Three-dimensional images were obtained with single cycle pulses at 40 MHz at the 3% power setting on the Vevo with an additional 20 dB attenuator in the transmission path. (This corresponded to a peak negative pressure of 38 kPa at the focus, as measured using a hydrophone.) The field of view of 0.98 mm × 0.98 mm was centered on the dot of microbubbles. The RF data were also acquired by an 8-bit A/D board and processed using Matlab (MathWorks Inc., Natick, MA) to derive reflected amplitudes. The frequency-dependent reflected amplitude was obtained by segmenting the surface reflection in the RF data, applying the Fourier transform and averaging results obtained around the center of the microbubble dot. This reflected amplitude was then compared with that of a quartz flat of known reflection coefficient ($R = 0.79$) to determine the absolute reflection coefficient of the surface. The reflected amplitude of a dot of microbubbles was also observed over time by scanning the surface at several minute intervals while keeping the surface submerged. The linearity of the reflected amplitude was also investigated by increasing the incident pressure. The potential disruption of microbubbles was investigated by exposing them to a series of 4500, one-cycle pulses (1 kHz PRF) and observing variations in the reflected amplitude. Linearity and disruption experiments were performed for negative peak pressures ranging from 38 to 440 kPa.

Simultaneously to the ultrasound scanning, the plates were observed with a custom-made dark-field adaptation of the Leica microscope at 20× magnification. Sample plates of bubbles were also observed under transmission light using an upright microscope with a 63× objective (NA = 0.9; Leica, Wetzlar, Germany,) for an estimation of the microbubble size distribution. The surface density of microbubbles was estimated using an image-processing code developed with Matlab, which was based on a thresholding and object-detection approach and compared with manual counting within a 5% error. Bubbles in samples of the solution were also counted and sized using a Coulter Multi-sizer 3 (Beckman Coulter Inc., Fullerton, CA) with an aperture of 20 μm, covering a range of 0.7 to 12 μm in diameter. The accuracy of both sizing methods (optical and Coulter) was determined using monodisperse latex size standard beads.

IV. Results

An optical microscope image of microbubbles bound on gelatin is shown in Fig. 3(a). The volume concentration of the dotted solution used for this image was about 100 million bubbles/mL. The microbubbles appeared as black dots with a diameter that could be resolved over 1 μm, which was twice the Abbe theoretical resolution limit for this microscope objective. Fig. 3(b) shows an example of microbubbles that were not distributed uniformly over the surface of gelatin. Such patterns were observed occasionally for very high surface densities of microbubbles and were not investigated with ultrasound.

The optical contrast between the microbubbles and the background allowed them to be counted. The relationship between the surface densities of microbubbles bound to the surface with respect to the concentration of microbubbles in the droplet is presented in Fig. 4. It shows that the number of bubbles on the surface increased with the total number of bubbles added.

The size distributions of microbubbles interrogated during the acoustical experiments superimposed with a lognormal best fit are presented in Fig. 5. The bound microbubbles had a maximum number fraction at a radius of 1.3 μm, and their distribution had a standard deviation of 0.57 μm as measured by the upright microscope. Less

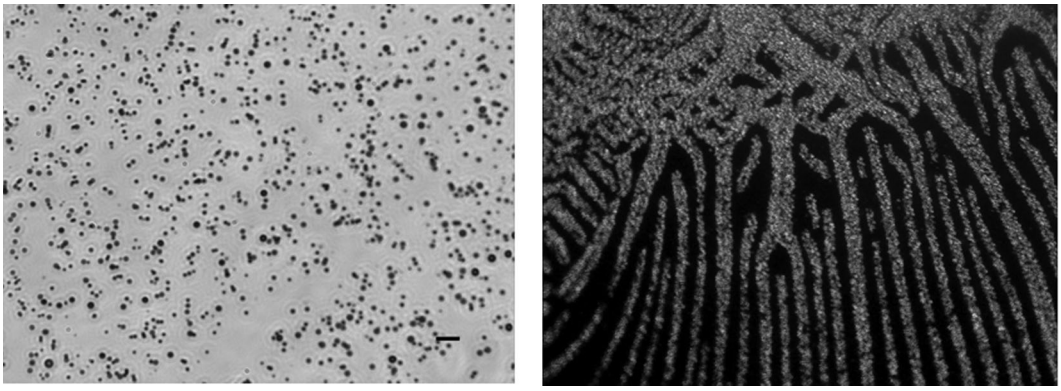

Fig. 3. (a) Bright-field microscope (40×) image of targeted microbubbles. The scale bar is 10 μm long. (b) Dark-field microscope (20×) picture of microbubbles forming a pattern at the edge of the dot.

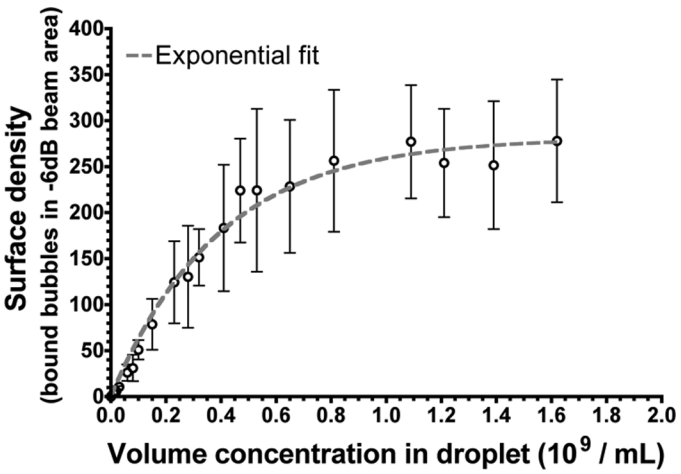

Fig. 4. Microbubbles binding efficacy. The error bars are standard deviations over different vials ($n = 4$) and the fit is an exponential ramp ($R^2 = 0.98$).

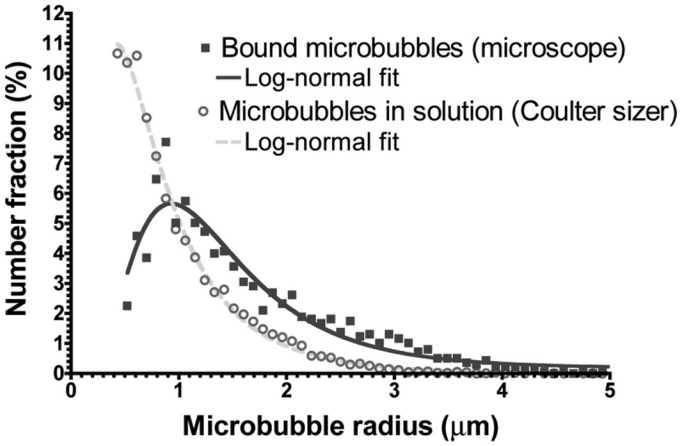

Fig. 5. Bubble size distribution as measured in solution by the Coulter counter ($n = 3$) and bound on a gelatin surface using an optical microscope. The fits are log-normal (Coulter: $R^2 = 0.99$, Microscope: $R^2 = 0.93$).

than 15% of all bound bubbles were larger than 2 μm in radius. The microbubbles measured in solution with the Coulter counter appeared smaller than their bound counterparts with a maximum number fraction at a radius of 0.7 μm and less than 5% of all bubbles bigger than 2 μm. Both optical and Coulter sizing methods appeared accurate with respect to the measurement of 2.12 μm (median) latex standard beads, which yielded 2.14 ± 0.16 μm and 1.97 ± 0.11 μm, respectively.

Results for the control experiments are shown in Figs. 6–8. As demonstrated by Fig. 6, the reflection from microbubbles bound to gelatin and immersed in degassed PBS was not constant over time but decreased to a quarter of its original value after 4 h. As expected, the reflection from the gelatin surface was independent of time. Fig. 7 shows the amplitude dependence of the reflection of microbubbles with respect to peak-negative pressure. As pressure was increased, the measured reflection coefficient deviated from the values found at 38 kPa. This effect is perceptible at 82 kPa and becomes significant at 140 kPa. Finally, the disruptive effects of 4500 ultrasound pulses on bound microbubbles are shown in Fig. 8. As the pressure amplitude of the repeated pulses increased, the reflection at the end of the disruption sequence decreased. No loss of signal was observed below 214 kPa.

The dots of microbubbles, as they appeared under a high-frequency ultrasound scanner, are shown in Fig. 9, with a field of view larger than used in the experiments. The presence of the microbubbles created bright disks of about 4 mm in diameter over the poorly reflective gelatin. During image acquisition, no microbubble detachment or free bubble was observed. Contrast was dependent on the surface density, measured by counting the microbubbles within the theoretical −6 dB transducer beam cross section in the focal plane. The beam area was estimated theoretically from the focal length and aperture and from the wavelength of the transmitted pulse. In general, the intensity of the reflections from the dots seemed to be uniform in the central part of the disk where the quantitative experiments were performed. However, it slightly increased over the edge as a consequence of higher microbubble densities.

Using the RF data acquired along the 2-D scan of the microbubble dots, the average reflection coefficient over

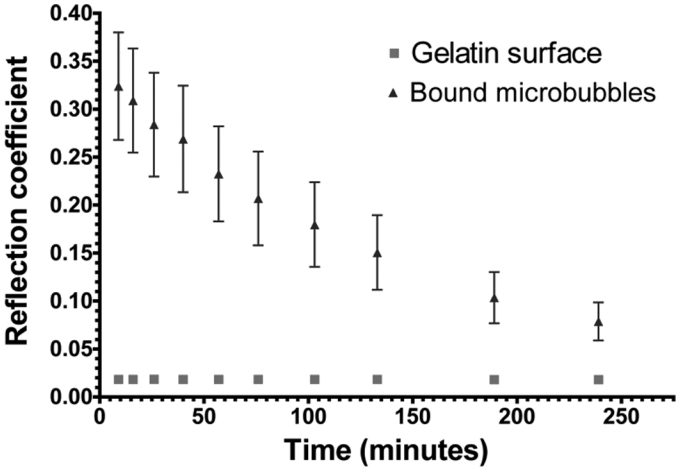

Fig. 6. Time evolution of the reflection of targeted microbubbles in PBS at room temperature (peak-negative pressure: 38 kPa). The error bars are standard errors ($n = 11$).

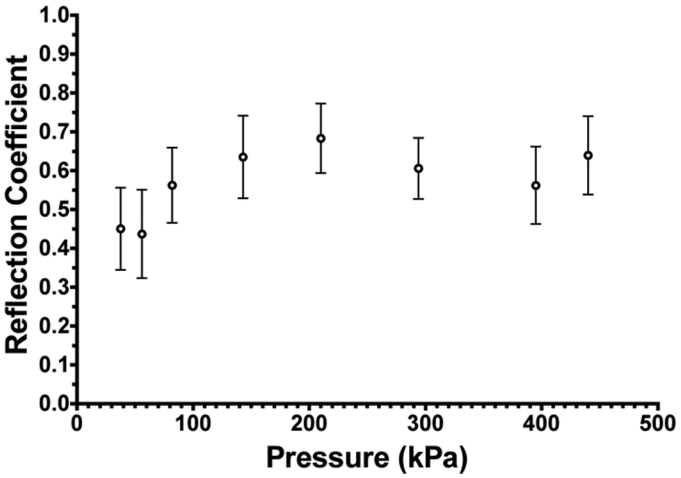

Fig. 7. Variation of the reflection from bound microbubbles at different incident peak negative pressures. The error bars are standard deviations ($n = 9$).

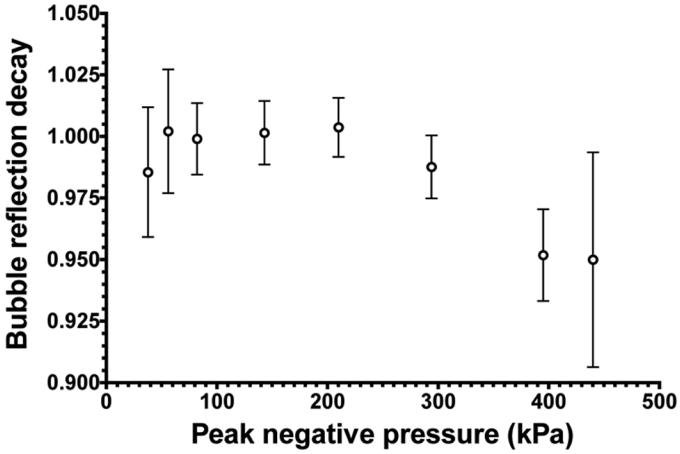

Fig. 8. Ratio between the reflection coefficient of bound microbubbles after and before 4500 single-cycle pulses at various amplitudes (1 kHz PRF). Error bars are standard deviations ($n = 9$).

the central part of each dot was estimated and is plotted in Fig. 10. Experimental data comprised 4 trials performed using different vials of the agent prepared before the experiments, each of which lasted approximately 45 min. All trials showed an increase in the reflection coefficient with an increase in the surface density up to a plateau of 0.9. This plateau, which was higher than the reflection coefficient from an acoustical mirror made of polished quartz ($r = 0.79$), was reached around 150 bound bubbles per beam area. Until 90 bubbles/per beam area, the reflection coefficient increased linearly with a slope of 0.0079 ± 0.0005 per bubble ($R^2 = 0.98$). For comparison, the reflection coefficient from the gelatin surface was 0.025.

Both the linear and multiple scattering models, derived from the theoretical model in Couture [20] and (6), respectively, are presented in Fig. 10. The scattering cross section of the microbubbles was derived from (1), which applies for linear scattering for long wavelengths and frequencies much higher than the resonance frequency of the bubbles. As a confirmation, this value was compared with the scattering cross section predicted by the Keller-Miksis [30] and Faran [31] models. It was found to be in agreement within 1% and 0.09%, respectively. Assuming negligible viscous damping in the bubble oscillation, the scattering function was calculated as a real number corresponding to the square root of the differential scattering cross section.

The linear model underestimated the increase in reflection coefficient for smaller number of microbubbles (slope: 0.005 per microbubble) and could not predict the reflection saturation. On the other hand, the multiple scattering model, which was only dependent on the size distribution of the bubbles and their surface density, provided a very good prediction of the reflection coefficient ($\chi^2 = 0.33$), because both the early increase and the plateau were correctly modeled.

V. Discussion

The goals of this study were to create a simple experimental system to study bound microbubbles, determine their acoustical properties under linear conditions, and compare results to a predictive model. Generally, microbubbles are assumed to have a nonlinear acoustical response, which is described by complex differential equations [21]. Linear models are not commonly used because they predict poorly the scattering of microbubbles near their resonance frequency, which contributes to a large fraction of backscattered signals in most clinical applications. The experimental results shown in Fig. 7 seem to demonstrate that at 40 MHz and at low pressures (under 50 kPa peak-negative), the behavior of these targeted microbubbles is amplitude independent. However, above 50 kPa, fluctuations in the reflection coefficient seem to indicate that bubbles might be undergoing oscillations resulting in nonlinear scattering. Nevertheless, the linearity

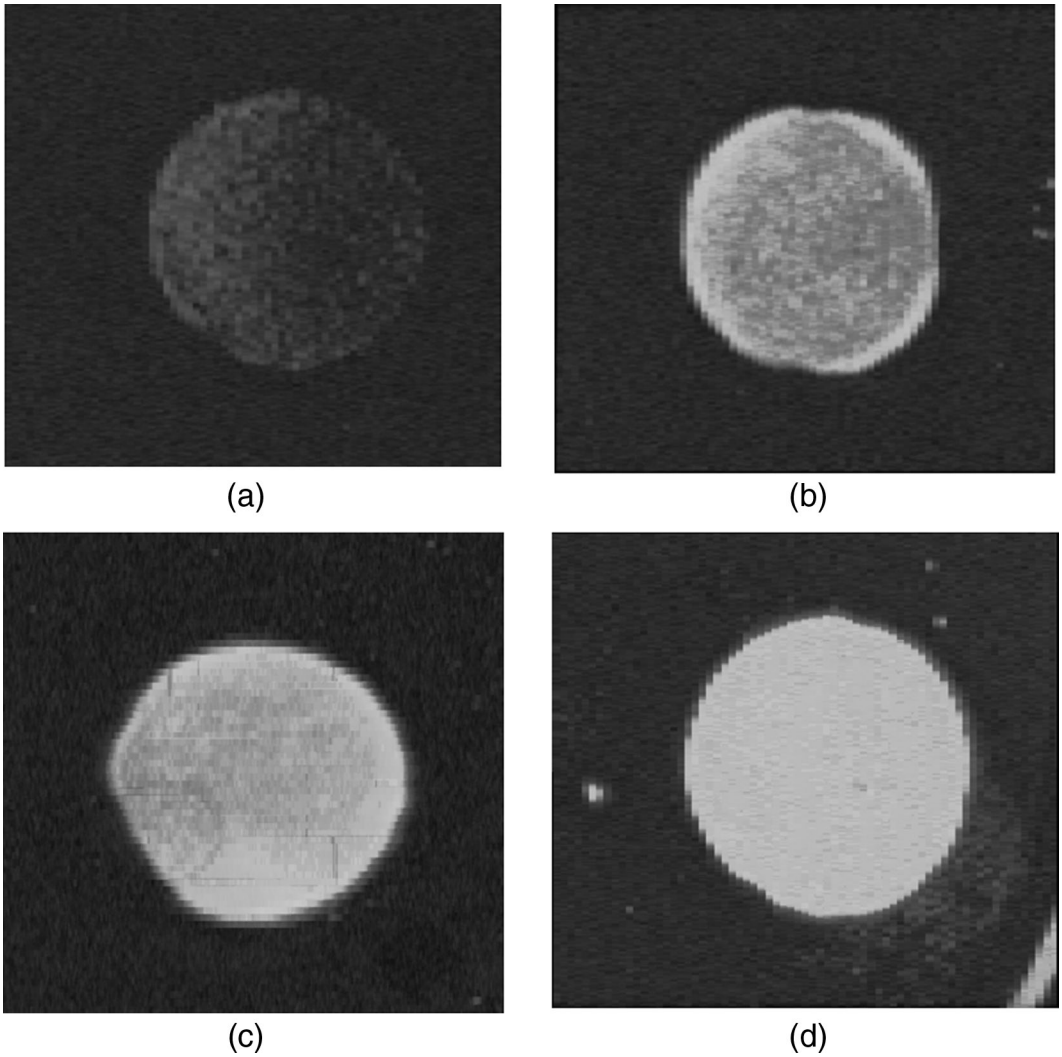

Fig. 9. C-Scan (40 MHz) of various concentrations of streptavidinated microbubbles on the gelatin surface. The field of view was extended to 6 mm × 6 mm. The surface density of microbubbles (in bound bubbles in −6 dB beam area) is 20 (A), 131 (B), 229 (C), and 331 (D).

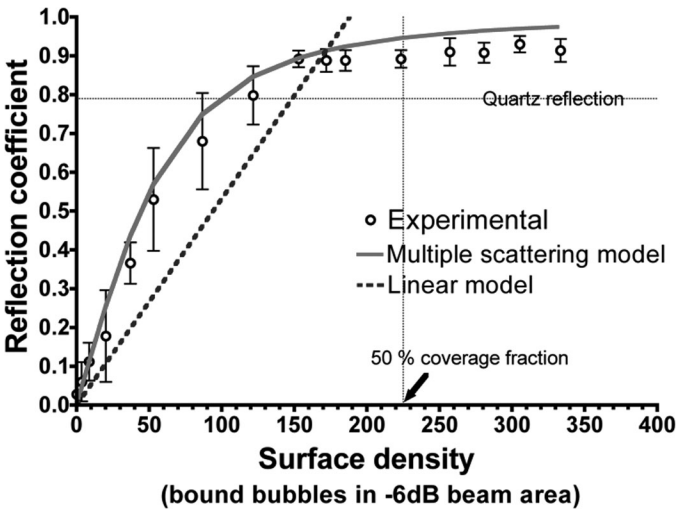

Fig. 10. Experimental and theoretical acoustic response of microbubbles bound on a gelatin surface at 40 MHz and with a 38 kPa peak-negative pressure. Error bars are standard deviations across different vials ($n = 4$). The linear and multiple scattering models were derived using the fitted size distribution measured by optical microscopy in Fig. 5.

assumption can be applied to the modeling of the behavior of populations in the conditions of the present study. However, calculations based on the work of Chin [22] show that multiple scattering has to be taken into account even when resonant microbubbles are separated by several diameters.

The initial experiments on binding microbubbles to a poorly reflective surface demonstrated that a gelatin surface is ideal for targeted bubble experiments. Acoustical properties of the gelatin surface can be modified by varying the concentration of gelatin dissolved in water to attain a reflection coefficient lower than 0.005. For simplicity, the microbubbles were not targeted using antibodies, but by relying on streptavidin's natural affinity for gelatin. Therefore, the binding was not specific. This may affect how the bubbles are bound to the surface and their response to acoustical waves. However, this simple experimental system provided sufficient stability for our preliminary purpose. As demonstrated by Figs. 3(a) and 4, many bubbles remained on the surface after multiple washes with PBS.

Not only are microbubbles strongly attached to the surface, but the number of bound bubbles is both reproducible and strongly dependent on the concentration of bubbles originally present in the solution (Fig. 4). Interestingly, the binding affinity decreases as the bubble density at the surface increased. In other words, a microbubble has less chance to bind when other microbubbles are already present. This seems to support the idea that microbubbles might interact repulsively, consequently preventing further binding in their proximity [32]. Such interactions between microbubbles might also explain the type of patterns observed in Fig. 3(b), which highlights the interesting problem of the fluid dynamics of microbubbles in very concentrated solutions.

The resolution of the microscope was sufficient to distinguish the borders of bubbles bigger than 1 μm in diameter. The resulting size distributions show that bound microbubbles had a fairly tight size distribution around 1.3 μm in radius, which was well described by a lognormal fit. Few bubbles were bigger than 2 μm in radius. Such a tight size distribution is advantageous for modeling the average backscattering of the bubble population. Interestingly, bound microbubbles are bigger than those observed in solution, which seems to contradict the results of Takalkar *et al.* who did not see any difference between the 2 populations [33]. Although the midpoint of microbubbles lying in different optical focal planes may introduce a systematic error of up to 5%, this does not fully account for the observed difference.

The experiments related to the reflectivity of surfaces were preceded by a series of experiments to determine the stability and the linearity of the signals reflected from microbubbles. The time stability experiment consisted of repeating the measurement of the reflection of 4 dots over 4 h. As shown in Fig. 6, the reflection of microbubbles in degassed PBS decreases significantly over time. This could introduce a systematic error even if the time between preparation and measurement is kept constant. In general, the stability of a bubble is strongly affected by its environment, such as a degassed solution or the capillary bed within lungs.

The assumption of linearity, which is fundamental to our modeling, was tested in Fig. 7. One-cycle pulses with different peak-negative pressures were incident on the microbubbles and the quartz to establish the variation in the reflection coefficient of the bound microbubbles. As the pressure was increased beyond 50 kPa, the reflection coefficient deviated significantly from the low-pressure value. In these conditions, microbubble scattering was no longer linear.

The last experiment was to determine if the microbubbles were affected by the experimental insonation. From Fig. 8, it can be seen that they are not affected by the low-pressure pulses (38 kPa), even after 4500 pulses. However, at higher pressures, the reflection of the microbubbles is reduced. This phenomenon was qualitatively observed in B-scan images of bound bubbles. This observation led to the use of the lowest transmission power of the Visualsonics Vevo 770 with an additional 20 dB of attenuation in transmission for the following experiments.

The ultrasound images of Fig. 9 show that the regions of enhanced reflection are confined and homogeneous, which supports the method of averaging the reflection over the dot. It also shows that the microbubbles are cleanly washed away from the surface. Thus, only the bound bubbles, initially in the dot, are present on the surface.

Fig. 10 shows that the reflection of a surface increases rapidly with the number of bound microbubbles. The initial slope demonstrates that the presence of 4 bubbles in the beam is sufficient to double the reflection coefficient of the gelatin surface, which eventually reaches a maximum of $R = 0.9$, a level higher than a polished surface of quartz, when as few as 150 microbubbles are present in the beam area. As a comparison, contrast agents made of liquid perfluorocarbon particles [20], [34] had a maximum reflection coefficient of 0.05, which is about 20 times lower than that of bound microbubbles for the same area coverage. Consequently, microbubbles should be preferred to liquid perfluorocarbon particles in applications requiring a high sensitivity of the ultrasound scanner to the targeted contrast agents, even in linear conditions, unless agent stability is a concern.

The reflection coefficient seems to be predicted accurately as a function of surface density by an adaptation of the model of Angel and Aristegui [26], which accounts for multiple scattering. Many simplifications can be made as assumptions are added, namely, isotropic scattering, long wavelength with respect to bubble size, frequencies much higher than the bubble resonance frequency, and uniform spatial distribution of the scatterers on the plane. The latter condition may become less valid as more microbubbles are accumulated on the gel surface. At high surface densities, the position of a microbubble will be influenced by the presence of its neighbors. This is demonstrated in Fig. 4, which shows that the binding of microbubbles depends on their concentration. Strictly speaking, our multiple scattering model is accurate only in the linear region of Fig. 4, until about 30,000 bubbles/mm^2. Above that limit, a quasi-crystalline term should be added to the model. It is difficult to assess if such surface densities are attainable *in vivo* because there are no standardized measurements for the densities of targeted contrast agents in such conditions. Intravital microscopy of microbubbles targeted to inflammation markers has shown that only a few bubbles per optical field are observable in a capillary bed [35], making multiple scattering unlikely. However, *in vitro* studies on aortic smooth muscle cells [36] and coronary artery endothelial cells [18] have shown that several particles can be targeted on single cells, leading to surface densities in the order of 1×10^3 microbubbles/mm^2. Such concentrations can induce multiple scattering, but are far from the upper bound of validity for the model presented in this study.

Fig. 10 demonstrates that the reflection coefficient cannot be fully described by summing linearly the contributions of individual microbubbles, as can be done for

particles with smaller scattering cross section [20], [37]. Moreover, these models do not scale with frequency. An increase in amplitude of the incident pulse, a decrease in its frequency or in the bubble size might cause the microbubbles to oscillate asymmetrically and undergo nonlinear oscillations. The use of higher frequencies to study populations of bound microbubbles makes possible many simplifications that would not apply at frequencies closer to resonance of microbubbles. For instance, because the scattering cross section of a microbubble is several orders of magnitude higher at the resonance frequency, multiple scattering should become notable at lower surface densities. Models taking the acoustical interactions between bubbles into account are thus even more important at clinical frequencies. However, the approximation that the scattering cross section is equal to the geometric cross section cannot be applied in such conditions and numerical simulations are required. Otherwise, the results from this study are directly applicable for higher frequency ultrasound applied to small animal [9] and intravascular imaging [36].

This study represents a first step in the modeling of the acoustical behavior of populations of bound microbubbles. Additional work should be done at lower frequencies to determine the limits of the model. In such a case, the scattering cross section should be obtained from nonlinear models such as Keller-Miksis, which are needed to describe the behavior of microbubbles closer to their resonance. More experiments are required to investigate the disruption level of bound microbubbles with respect to their free-flowing counterparts and the behavior of single bound microbubbles. Finally, the study of the reflection coefficient of targeted microbubbles should be extended to clinically relevant situations, such as endothelial cell surfaces and thrombi.

VI. Conclusion

This study measured and modeled the echo from targeted microbubbles at high frequencies. A simple experiment was used to measure the reflection coefficient at 40 MHz from microbubbles bound to a poorly reflective surface. Control experiments show that the reflection of targeted microbubbles is linear for single-cycle pulses below 140 kPa peak-negative pressure at this frequency. The reflection coefficient of microbubbles correlated well with the number of microbubbles on the surface measured with optical microscopy. The maximum reflection coefficient, R, was measured to attain a value of 0.9 when 35% of the surface was covered with the agent. These values were predicted by a multiple scattering model, which was valid for the high frequency and low powers used in our experiments. These results may contribute to the optimization of parameters, such as the required dose of agent for detection of a specific receptor, which is a critical parameter for targeted microbubble imaging.

Appendix

The average distance to the closest particle on a surface (r_{mean}) can be determined from the surface density (n_S) using a modified version of the calculation given by Chin [22].

Assuming that particles are independently placed over a surface, the probability that x bubbles are found within an area A of the surface around another bubble is given by the Poisson distribution:

$$P(x) = \frac{e^{-n_S A}(n_S A)^x}{x!}.$$

The probability density that the nearest neighboring particle is between a radius of r and $r + dr$ can then be expressed as the following product:

$$f(r)dr = P(0)_{\text{ within } A} P(1)_{\text{ within } (A+dA)} = e^{-n_S A} e^{-n_S dA}(n_S dA).$$

Simplifying using the following definitions

$$A = \pi r^2$$

$$dA = 2\pi r dr$$

$$r_o{}^2 = \frac{1}{\pi n_S}$$

yields

$$f(r) = \frac{2r}{r_o} e^{-r^2/r_o{}^2}.$$

The average distance to the next particle can be obtained from the following integral:

$$r_{\text{mean}} = \int_0^\infty r f(r) dr = \frac{2}{r_o{}^2}\int_0^\infty r^2 e^{-r^2/r_o{}^2} dr$$

$$= \frac{\sqrt{\pi r_o{}^2}}{2} = \frac{1}{2}\sqrt{\frac{1}{n_S}}.$$

Acknowledgments

The authors thank Bracco Research SA for providing the microbubbles. The authors also thank Valentin Leroy (Laboratoire Ondes et Acoustique, Paris) for fruitful discussions.

References

[1] P. A. Dayton and J. J. Rychak, "Molecular ultrasound imaging using microbubbles contrast agent," *Front. Biosci.*, vol. 12, pp. 5124–5142, Sep. 2007.

[2] K. W. Ferrara, C. R. B. Merritt, P. N. Burns, F. S. Foster, R. F. Mattrey, and S. A. Wickline, "Evaluation of tumor angiogenesis with US: Imaging, Doppler and contrast agents," *Acad. Radiol.*, vol. 7, pp. 824–839, Oct. 2000.

[3] D. Cosgrove, "Angiogenesis imaging—Ultrasound," *Br. J. Radiol.*, vol. 76, spec. no. 1, pp. S43–S49, 2003.
[4] D. B. Ellegala, H. Leong-Poi, J. E. Carpenter, A. L. Klibanov, S. Kaul, M. E. Shaffrey, J. Sklenar, and J. R. Lindner, "Imaging tumor angiogenesis with contrast ultrasound microbubbles targeted to alpha-v-beta-3," *Circulation*, vol. 108, pp. 336–341, Jul. 2003.
[5] H. Leong-Poi, J. Christiansen, P. Heppner, C. W. Lewis, A. L. Klibanov, S. Kaul, and J. R. Lindner, "Assessment of endogeneous and therapeutic arteriogenesis by contrast ultrasound molecular imaging of integrin expression," *Circulation*, vol. 111, pp. 3248–3254, Jun. 2005.
[6] P. M. Winter, A. M. Morawski, S. D. Caruthers, R. W. Furhop, H. Zhang, T. S. Williams, J. S. Allen, E. K. Lacy, J. D. Robertson, G. M. Lanza, and S. A. Wickline, "Molecular imaging of angiogenesis in early-stage atherosclerosis with alpha-v-beta-3-integrin targeted nanoparticles," *Circulation*, vol. 108, pp. 2270–2274, Nov. 2003.
[7] J. K. Willmann, R. Paulmurugan, K. Chen, O. Gheysens, M. Rodriguez-Porcel, A. M. Lutz, I. Y. Chen, X. Chen, and S. S. Gambhir, "US imaging of tumor angiogenesis with microbubbles targeted to vascular endothelial growth factor receptor Type 2 in mice," *Radiology*, vol. 246, pp. 508–518, Feb. 2008.
[8] A. Lyshchik, A. C. Fleischer, J. Huamani, D. E. Hallahan, M. Brissova, and J. C. Gore, "Molecular imaging of vascular endothelial growth factor receptor 2 expression using targeted contrast-enhanced high-frequency ultrasonography," *J. Ultrasound Med.*, vol. 26, pp. 1575–1586, Nov. 2007.
[9] J. J. Rychak, J. Graba, A. M. Cheung, B. S. Mystry, J. R. Lindner, R. S. Kerbel, and F. S. Foster, "Microultrasound molecular imaging of vascular endothelial growth factor receptor 2 in a mouse model of tumor angiogenesis," *Mol. Imaging*, vol. 6, pp. 289–296, Sep.–Oct. 2007.
[10] J. J. Rychak, A. L. Klibanov, K. F. Ley, and J. A. Hossack, "Enhanced targeting of ultrasound contrast agents using acoustic radiation forces," *Ultrasound Med. Biol.*, vol. 33, pp. 1132–1139, Jul. 2007.
[11] J. R. Lindner, J. Song, J. Christiansen, A. L. Klibanov, F. Xu, and K. Ley, "Ultrasound assessment of inflammation and renal tissue injury with microbubbles targeted to P-selectin," *Circulation*, vol. 104, pp. 2107–2112, Oct. 2001.
[12] G. M. Lanza, K. D. Wallace, M. J. Scott, W. P. Cacheris, D. R. Abendschein, D. H. Christy, A. M. Sharkey, J. G. Miller, P. J. Gaffney, and S. A. Wickline, "A novel site-targeted ultrasonic contrast agent with broad biomedical application," *Circulation*, vol. 94, pp. 3334–3340, Dec. 1996.
[13] P. A. Schumann, J. P. Christiansen, R. M. Quigley, T. P. McCreery, R. H. Sweitzer, E. C. Unger, J. R. Lindner, and T. O. Matsunaga, "Targeted-microbubble binding selectively to GPIIb IIIa receptors of platelet thrombi," *Invest. Radiol.*, vol. 37, pp. 587–593, Nov. 2002.
[14] P. N. Burns and S. R. Wilson, "Microbubble contrast for radiological imaging: 1. Principles," *Ultrasound Q.*, vol. 22, pp. 5–13, Mar. 2006.
[15] N. de Jong, A. Bouakaz, and P. Frinking, "Basic acoustic properties of microbubbles," *Echocardiography*, vol. 19, pp. 229–240, Apr. 2002.
[16] V. Garbin, E. Ferrari, D. Cojoc, E. Di Fabrizio, M. I. J. Overvelde, S. M. van der Meer, and M. Versluis, "Optical trapping of ultrasound contrast microbubbles," in *Proc. IEEE Ultrasonics Symp.*, 2006, pp. 513–516.
[17] S. Zhao, K. W. Ferrara, and P. A. Dayton, "Asymmetric oscillation of adherent targeted ultrasound contrast agents," *Appl. Phys. Lett.*, vol. 87, art. no. 134103, Dec. 2005.
[18] F. S. Villanueva, R. J. Jankowski, S. Klibanov, M. L. Pina, S. M. Alber, S. C. Watkins, G. H. Brandenburger, and W. R. Wagner, "Microbubbles targeted to intercellular adhesion molecule-1 bind to activated coronary artery endothelial cells," *Circulation*, vol. 98, pp. 1–5, Jul. 1998.
[19] M. Lankford, C. Z. Behm, J. Yeh, A. L. Klibanov, P. Robinson, and J. R. Lindner, "Effect of microbubble ligation to cells on ultrasound signal enhancement: Implications for targeted imaging," *Invest. Radiol.*, vol. 41, pp. 721–728, Oct. 2006.
[20] O. Couture, P. D. Bevan, E. Cherin, K. Cheung, P. N. Burns, and F. S. Foster, "A model for reflectivity enhancement due to surface bound submicrometer particles," *Ultrasound Med. Biol.*, vol. 32, pp. 1247–1255, Aug. 2006.
[21] S. Hilgenfeldt, D. Lohse, and M. Zomack, "Response of bubbles to diagnostic ultrasound: A unifying theoretical approach," *Eur. Phys. J. B*, vol. 4, no. 2, pp. 247–255, 1998.
[22] C. T. Chin and P. Burns, "Modelling the behaviour of microbubble contrast agents for diagnostic ultrasound," Ph.D. dissertation, Dept. of Medical Biophysics, Univ. Toronto, Toronto, Canada, 2001.
[23] L. L. Foldy, "The multiple scattering of wave," *Phys. Rev.*, vol. 67, no. 3-4, pp. 107–119, 1943.
[24] E. L. Cartensen and L. L. Foldy, "Propagation of sound through a liquid containing bubbles," *J. Acoust. Soc. Am.*, vol. 19, no. 3, pp. 481–501, 1947.
[25] P. C. Waterman and R. Truell, "Multiple scattering of waves," *J. Math. Phys.*, vol. 2, no. 4, pp. 512–537, 1961.
[26] Y. C. Angel and C. Aristegui, "Analysis of sound propagation in a fluid through a screen of scatterers," *J. Acoust. Soc. Am.*, vol. 118, no. 1, pp. 72–82, 2005.
[27] L. Y. L. Mo and R. S. C. Cobbold, "A unified approach to modeling the backscattered Doppler ultrasound from blood," *IEEE Trans. Biomed. Eng.*, vol. 39, pp. 450–461, May 1992.
[28] C. Feuillade and C. S. Clay, "Anderson (1950) revisited," *J. Acoust. Soc. Am.*, vol. 106, no. 2, pp. 553–564, 1999.
[29] C. X. Deng and F. L. Lizzi, "A review of physical phenomena associated with ultrasonic contrast agents and illustrative clinical applications," *Ultrasound Med. Biol.*, vol. 28, pp. 277–285, Mar. 2002.
[30] J. B. Keller and M. Miksis, "Bubble oscillations at large amplitude," *J. Acoust. Soc. Am.*, vol. 68, no. 2, pp. 628–633, 1980.
[31] J. J. Faran, "Sound scattering by solid cylinders and spheres," *J. Acoust. Soc. Am.*, vol. 24, no. 4, pp. 405–418, 1951.
[32] A. L. Klibanov, "Ultrasound contrast agents: Development of the field and current status," *Top. Curr. Chem.*, vol. 222, pp. 74–106, 2002.
[33] A. M. Takalkar, A. L. Klibanov, J. J. Rychak, J. R. Lindner, and K. Ley, "Binding and detachment dynamics of microbubbles targeted to P-selectin under controlled shear flow," *J. Control. Release*, vol. 96, pp. 473–482, May 2004.
[34] G. M. Lanza, R. L. Trousil, K. D. Wallace, J. H. Rose, C. S. Hall, M. J. Scott, J. G. Miller, P. R. Eisenberg, P. J. Gaffney, and S. A. Wickline, "In vitro characterization of a novel, tissue-targeted ultrasonic contrast system with acoustic microscopy," *J. Acoust. Soc. Am.*, vol. 104, no. 6, pp. 3665–3672, 1998.
[35] J. R. Lindner, M. P. Coggins, S. Kaul, A. L. Klibanov, G. H. Brandenburger, and K. Ley, "Microbubble persistance in the microcirculation during ischemia/reperfusion and inflammation is caused by integrin- and complement mediated adherence to activated leukocytes," *Circulation*, vol. 101, pp. 668–675, Feb. 2000.
[36] G. M. Lanza, D. R. Abendschein, C. S. Hall, J. N. Marsh, M. J. Scott, D. E. Scherrer, and S. A. Wickline, "Molecular imaging of stretch-induced tissue factor expression in carotid arteries with intravascular ultrasound," *Invest. Radiol.*, vol. 35, pp. 227–234, Apr. 2000.
[37] O. Couture, E. Cherin, and F. S. Foster, "Model for the ultrasound reflection from micro-beads and cells distributed in layers on a uniform surface," *Phys. Med. Biol.*, vol. 52, pp. 4189–4204, Jul. 2007.

Olivier Couture was born in Quebec City, Canada, in 1978. He received his B.Sc. degree in physics from McGill University, Montreal, Canada, in 2001, and his Ph.D. degree from the Department of Medical Biophysics, University of Toronto, Canada, in 2007. He is now doing postdoctoral studies at the Laboratoire Ondes et Acoustique at the ESPCI in Paris, France. His current research interests include targeted ultrasound contrast agents, HIFU, nonlinear acoustics, drug encapsulation, and French cuisine.

Michael Roger Sprague was born in Toronto in 1985. Having graduated in 2007 with a B.A.Sc. degree in engineering physics at Queen's University, he is continuing his training by working toward an M.S. degree at the Department of Medical Biophysics at the University of Toronto. His current research interests encompass the application of targeted contrast agents to high-frequency ultrasound and the evolution of highly dynamic systems.

Emmanuel Cherin received a Ph.D. degree in physical acoustics from the University Paris VI, Paris, France, in 1998. Soon after, he joined the imaging research group at the Sunnybrook Health Sciences Centre, Toronto, ON, Canada, as a postdoctoral fellow. Since 2001, he has occupied a position as research associate with the ultrasound group, where he is involved in projects related in particular to high-frequency transducer characterization, nonlinear acoustics, and contrast agent imaging

Peter N. Burns is chair of the Department of Medical Biophysics and professor of radiology at the University of Toronto and senior scientist at Sunnybrook Health Sciences Centre, Toronto. He received his Ph.D. degree in radiodiagnosis at the University of Bristol, Bristol, UK. His main interest is blood flow detection and instrumentation for Doppler ultrasound, including detecting blood flow in tumors and other small vessel systems. His most recent work is with color Doppler instrumentation, hemodynamic measurement with Doppler and, most recently, ultrasound contrast agents and the development of harmonic imaging.

F. Stuart Foster received a Ph.D. degree from the University of Toronto in 1980 and is currently professor and Canada Research Chair in Ultrasound Imaging, Department of Medical Biophysics, University of Toronto. Dr. Foster is a former Terry Fox Scientist of the National Cancer Institute of Canada and has been involved with the development of new ultrasonic imaging systems since 1975. He has made contributions to the development of systems for the detection and evaluation of prostate, breast, and ocular cancers. His current research centers on the development of high-frequency clinical and preclinical imaging systems, array technology, intravascular imaging, and molecular imaging. He was the 1995–1996 Distinguished Lecturer for the IEEE (UFFC). In 1997, he won the Thomas Eadie Medal for major contributions to engineering and applied science in Canada from the Royal Society of Canada. He is a fellow of the American Institute of Ultrasound in Medicine. In 1999, he founded VisualSonics, a company aimed at preclinical mouse imaging, and he remains its chief scientific officer. Dr Foster co-founded the Mouse Imaging Centre (MICe) at the Toronto Centre for Phenogenomics. He has served on the board of directors of the National Cancer Institute of Canada and as chairman of its Committee on Research (ACOR). He has recently been the recipient of the Queen's Golden Jubilee Medal, the Manning Award of Distinction for Canadian Innovation, and the Ontario Premier's Discovery Award. He serves on numerous advisory bodies and is currently on the editorial boards of *Ultrasonic Imaging* and *Ultrasound in Medicine and Biology*.